Specific separation and recovery of phosphate anions by a novel NiFe-LDH/rGO hybrid film based on electroactivity-variable valence

Pengfei Ma[1,4*], Jiangwei Zhu[1], Xiao Du[1], Yanyan Yang[2], Xiaoqiong Hao[3], Xiaowei An[1], Xiaogang Hao[1*], Claudia Prestigiacomo[4]

1. Department of Chemical Engineering, Taiyuan University of Technology, Taiyuan 030024, China

2. School of Chemistry and Environmental Science, Shangrao Normal University, Shangrao 334001, China

3. Jiangsu Key Laboratory of Advanced Catalytic Materials and Technology Changzhou University, Changzhou 213164, China

4. Dipartimento di Ingegneria, Università Degli Studi di Palermo, Palermo 90128, Italy

Corresponding authors:

E-mail addresses: xghao@tyut.edu.cn (X. Hao); mapengfei01@tyut.edu.cn (P. Ma).

Abstract: Phosphorus is a non-renewable resource. Supplies are limited and much phosphorus is currently wasted during the production and utilization process, causing concerns about future supplies and widespread environmental problems. In order to solve these problems, a new type of NiFe-LDH/rGO electrically switched ion-selective (ESIX) film is designed, based on the dominant mechanism of inner-sphere complexation. An ESIX process allows the NiFe-LDH/rGO hybrid film achieving a controllably selective uptake and release of the phosphate anions. This route involves tuning potential steps to regulate the redox states of the composite film and the variable metal (e.g., Ni, Fe (II)/(III)) in coordination centers, as the inner-sphere complexation of the metals to phosphate anions is combined with the assistance of the outer electric field. A high absorption capacity (270 mg$\cdot$g^{-1}) and regeneration rate (>85%) were achieved, together with good cycle stability.

Keywords: phosphate anions; layered double hydroxides; valence state transition; inner-sphere complexation; adsorption capacity; selective extraction.

1. Introduction

Excessive phosphate discharge in water environments leads to eutrophication, which is one of the most widespread global problems on water quality (Velusamy et al., 2021). Various technologies including chemical precipitation (Sun et al., 2020), enhanced biological process (Wu, Lo et al., 2020), and adsorption processes (Wu, Wan et al., 2020) have been studied to remove the phosphate pollutants from water. However, these commonly adopted technologies still face some bottlenecks. Through chemical precipitation, for example, the phosphate pollutants were separated from water because their precipitation was induced adding to the system large amount of chemicals, resulting in secondary pollution (Hassan et al., 2020). While the phosphorus removal by enhanced biological process usually is characterized by low operation stability, high treatment costs and strong dependence on environmental factors, that make difficult to adapt the process to the stringent regulations on phosphate limits in water (Zou et al., 2016).

Selective adsorption constitutes an advanced phosphorus removal technology as it is a direct and effective recovery route. However, the selective adsorption of phosphate is challenging to realize. On the one hand, the removal efficiency of phosphate by commonly used adsorbents is low due to the high hydration energy of phosphate and the existence of the competitive anions in the water, which lead to low purity of phosphate recovery solution obtained by adsorbent regeneration (Wu et al., 2017). On the other hand, the adsorption method mainly relies on the concentration gradient to drive the ion transfer, which is limited by the diffusion control process (Gu et al., 2007),

65 resulting in adsorption and desorption efficiency being slow and time-consuming.

66 Moreover, the use of chemical elution reagent in the regeneration process of adsorbent

67 often cause a secondary pollution (Yang et al., 2018).

68   As we all know, adsorbents are exstensively involved in investigations to improve

69 the efficiency of adsorption technology. The enhancement of uptake and release

70 capabilities of an ideal adsorbent requires understanding the changes of phosphate

71 bonds during uptake/release process. It has been found that the outermost electron and

72 vacancy molecular orbital are responsible for the interaction and bonding ability

73 between ions. Compared with other coexisting anions (such as SO_4^{2-}, NO_3^- and Cl^-),

74 phosphate anions has a higher ability to provide isolated electron pairs, In particular,

75 the adsorption process of phosphate anions can be realized by forming an inner sphere

76 complex with metal-based adsorbent (ligand exchange between phosphate and surface

77 hydroxyl) (Morimoto et al., 2012). After that, the desorption process is realized by using

78 alkaline solutions such as NaOH (Nuryadin et al., 2021) and the adsorbed phosphate

79 anions will be replaced by OH^-. In view of this, layered double hydroxides (LDHs),

80 with different metal hydroxide layers and anion and water molecular space, are one of

81 the most potential electro-adsorption materials for the selective removal of phosphate

82 pollutants (Liu et al., 2019).

83   To date, there are some studies focused on phosphate removal using LDHs. For

84 example, Hong et al. prepared the ZnAl-layered double hydroxide (LDH) with reduced

85 graphene oxide (LDH/rGO) composite to selectively remove phosphate by capacitive

86 deionization process, as a result, LDH/rGO showed a decrease of the concentration of

87   phosphate from 0.4 mg·L^{-1} to 0.009 mg·L^{-1} (Hong et al., 2019). Meanwhile, Rahman et

88   al. investigated the utilization of Fe/Mg-LDH disp

89   ersed on biochar for the phosphate recovery process. In particular they found high

90   capacities of phosphate adsorption for both LDH and LDH-modified biochar (i.e. from

91   154 to 241 mg·g^{-1} and from 117 to 1589 mg·g^{-1} respectively) (Rahman et al., 2021).

92   With these premises, it is possible to understand that phosphate selective adsorption

93   performances can be achieved. However, the outcomes of the literature demonstrated

94   that the process was characterized by low adsorption and desorption efficiencies, and

95   the separation of phosphate in low concentration it is difficult to achieve. Hence, the

96   way to design a promising adsorbent and adopt a competitive technology is significant.

97   The ESIX developed by our research group is a new seawater/wastewater

98   desalination technology (Niu et al., 2020). In this technology, the functional material is

99   deposited on the conductive matrix in a certain way to prepare the film electrode

100   material, and the redox potential on the film electrode material is controlled by using

101   the electrochemical method, so as to achieve the reversible uptake/release of the target

102   ion in the solution system, and achieve the efficient separation of the target ions.

103   Compared with traditional phosphorus removal technology, the regeneration process

104   does not need to add chemical cleaning agents, no secondary pollution, suitable for

105   selective separation of low concentration target ions (Du et al., 2016).

106   This study examines the utilization of a novel electrochemically switched ion

107   exchange film for selective separation and recovery of phosphate anions. A NiFe-LDH

108 (M stands for Ni or Fe) with reduced graphene oxide (LDH/rGO) was prepared, in

109 which the rGO not only improves the conductivity of the hybrid film and provids a

110 convenient channel for electron conduction, so as to effectively regulate the redox

111 potential on the hybrid film, realized the uptake and release of phosphate anions, but

112 also greatly disperses the LDH sheet and exposes more of its adsorption sites. A

113 systematic analysys was carried out in order to evaluate the synergistic effects of the

114 hybrid film, the effects of the redox state of the composite film ($NiFe^{2+}/NiFe^{3+}$), the

115 selective adsorption of phosphate anions and the regeneration efficiency of the hybrid

116 film, the efficiency of removal of phosphate anions in low concentrated solutions, the

117 regeneration of the hybrid film, the effects of changes of the pH of the solution. It is

118 found that the hybrid film has excellent selective adsorption and desorption to

119 phosphate anions by using ESIX technology under potential regulation, and the

120 adsorption capacity reaches as high as about 270 mg·g^{-1}.

121 **2. Experimental section**

122 **2.1 Material synthesis**

123   Firstly, the GO nanosheets were obtained by placing 80 mg GO powder in 200 mL

124 of deionized aqueous solution and ultrasonic oscillation for 2 h. Secondly, 18 mmol

125 $Ni(NO_3)_2·6H_2O$, 6 mmol $Fe(NO_3)_3·9H_2O$ and 0.3 mol urea were added to GO

126 dispersion in solution, then it was stirred for 30 min. The mixed solution was placed in

127 a high-pressure reactor with a reaction temperature of 95°C and a heating time of 24 h.

128 The obtained precipitate was centrifuged and washed until the solution was neutral

129 (pH=7), and then it was dried in a vacuum freeze-drying oven for 12 h to obtain NiFe-

130   LDH/GO.

131   The NiFe-LDH/rGO hybrid material was obtained by the thermochemical

132   reduction method. The NiFe-LDH/GO was placed in a beaker and then placed in a

133   reaction kettle containing 500 µl hydrazine hydrate. After heating and reducing at 90°C

134   for 24 h, the obtained substance was removed and placed in a vacuum drying box at

135   60°C for 12 h to obtain NiFe-LDH/rGO hybrid material.

136   **2.2 Electrode fabrication**

137   The NiFe-LDH/rGO hybrid film was prepared by the coating method. The NiFe-

138   LDH/rGO hybrid material, PVDF and conductive carbon black were dissolved in the

139   NMP solution at a mass ratio of 8:1:1. The solution was stirred overnight to promote

140   the mixing of the three compounds. Subsequently, the hybrid film can be obtained by

141   coating on the conductive titanium network and then put into the oven at 40°C overnight.

142   **2.3 Extraction performance and electrochemical tests**

143   The extraction performance and electrochemical tests were performed by a three-

144   electrode system (working electrode: NiFe-LDH/rGO hybrid film; counter electrode: 2

145   mm thick graphite paper; reference electrode: Ag/AgCl). The electrochemical activity

146   of NiFe-LDH/rGO hybrid film were measured by cyclic voltammetry (CV). The

147   extraction capacities of NiFe-LDH/rGO hybrid film for phosphate anions at different

148   concentrations (100, 200, 300 and 500 ppm) were investigated by potentiostatic method

149   (CA), where the adsorption voltage was set as 0.8 V. Different pH (3-11) effect were

150   tested in sodium dihydrogen phosphate solution of 300 ppm.

151    $$Q = \frac{(C_0 - C_e) \times V}{M} \tag{1}$$

152   Eq. (1) is the calculation equation of adsorption capacity of hybrid film for

153   phosphate anion. Where C_0 (mg·L^{-1}) and C_e (mg·L^{-1}) is the initial concentration and the

154   equilibrium concentration of the electrolyte solution (i.e., sodium phosphate solution),

155   respectively; V (L) is the initial volume of electrolyte solution; M (g) is the net mass of

156   the film after removing the titanium mesh.

157    $$K_D = \frac{C_0 - C_e}{C_e} \times \frac{V}{M}$$ (2)

158    $\alpha = K_D(PO_4^{3-})/K_D(\text{others anions})$ (3)

159   In addition, to explore the selection performance of NiFe-LDH/rGO hybrid film

160   for phosphate anion, the adsorption capacity of different anions (Cl$^-$, NO$_3^-$, SO$_4^{2-}$ and

161   PO$_4^{3-}$) in 300 ppm solution was investigated. Eq. (2) and Eq. (3) were used to calculate

162   the adsorption selectivity of the hybrid film for phosphate anion in the presence of

163   different competing anions. Where K_D (ml·g^{-1}) is the distribution coefficient; α is the

164   ratio of the separation coefficient of phosphate anion to that of other anions; C_0 (mg·L^{-1}

165   ^{1}), Ce (mg·L^{-1}) is the initial concentration of the electrolyte solution and the

166   concentration at equilibrium, respectively; M and V are the same as Eq. (1).

167   All the experimental data were tested for three times, and the average value was

168   calculated.

169   **2.3 Density functional theory (DFT) Calculations**

170   In order to further explore the excellent adsorption selectivity of the NiFe-LDH to

171   phosphate anions. The binding energies of different anions with NiFe-LDH were

172   calculated DFT Calculation using DMOL3 module in Accelrys Material Studio 8.0

173   (AMS) package. The generalized gradient approximation (GGA), Perdew-Burke-

174 Ernzerhof exchange correlation function (PBE) and double numerical orbital basis set

175 (DNP) were used (Tipplook et al., 2021).

3. Results and discussion

177   The preparation process of NiFe-LDH/rGO hybrid film and the mechanism of

178 phosphate anions uptake/release were shown in Scheme 1. The mixed solution

179 containing nickel and iron ions was evenly dispersed in the solution containing GO

180 nanosheets. Urea was used to provide an alkaline environment. Then, the NiFe-

181 LDH/GO hybrid film was prepared at 95°C. The obtained hybrid film was reduced by

182 hydrazine hydrate steam to obtain the NiFe-LDH/rGO hybrid material, mixing with

183 PVDF and conductive carbon black in a certain proportion and coated on conductive

184 titanium net to obtain the NiFe-LDH/rGO hybrid film. Interestingly, the LDH sheet was

185 tiled on the GO nanosheet prepared hybrid material in the preparation process. However,

186 the LDH sheet grew at a different angle on the rGO, instead of tiled on the GO. This

187 phenomenon could provide convenient conditions for ions transport and play a

188 significant role in promoting the reversible ion placement and removal of the material,

189 which could be proved by Fig.1 and verified by Tian et al. report (Tian et al., 2019).

190   Scheme 1 describes the mechanism of uptake and release of phosphate anions by

191 the mixed film. Firstly, an appropriate positive potential was given to the film electrode,

192 resulting in an oxidation state, and electrons will transfer from the LDH（A）to the

193 surface of rGO (B), then transmitting to the power (D) supply through the titanium

194 mesh (C) (e$^-$: A→B→C→D). In the meantime that the corresponding electroactive

195 substance was activated, bivalent nickel and iron ions would have been oxidized into

196 trivalent ($Ni^{2+}/Fe^{2+} \rightarrow Ni^{3+}/Fe^{3+}$). To balance the loss of interlayer anions, phosphate

197 anions would be inserted to compensate for the charge loss. On the contrary, at a

198 negative potential, the composite film electrode was in a reduced state, and the electrons

199 transferred from the power source to the titanium mesh, the reduction of the graphene

200 oxide surface, and to the corresponding active material (e^-: D→C→B→A). The

201 Ni^{3+}/Fe^{3+} would be reduced to Ni^{2+}/Fe^{2+} in the composite film electrode at the reduced

202 state. At this time, the excess phosphate anions between the LDH layers and the

203 substrate would be desorbed and released into the solution to balance the excess charge

204 between the layers. Therefore, the reversible uptake and release of phosphate ions could

205 be achieved by changing the redox potential of the hybrid film in the process of ESIX.
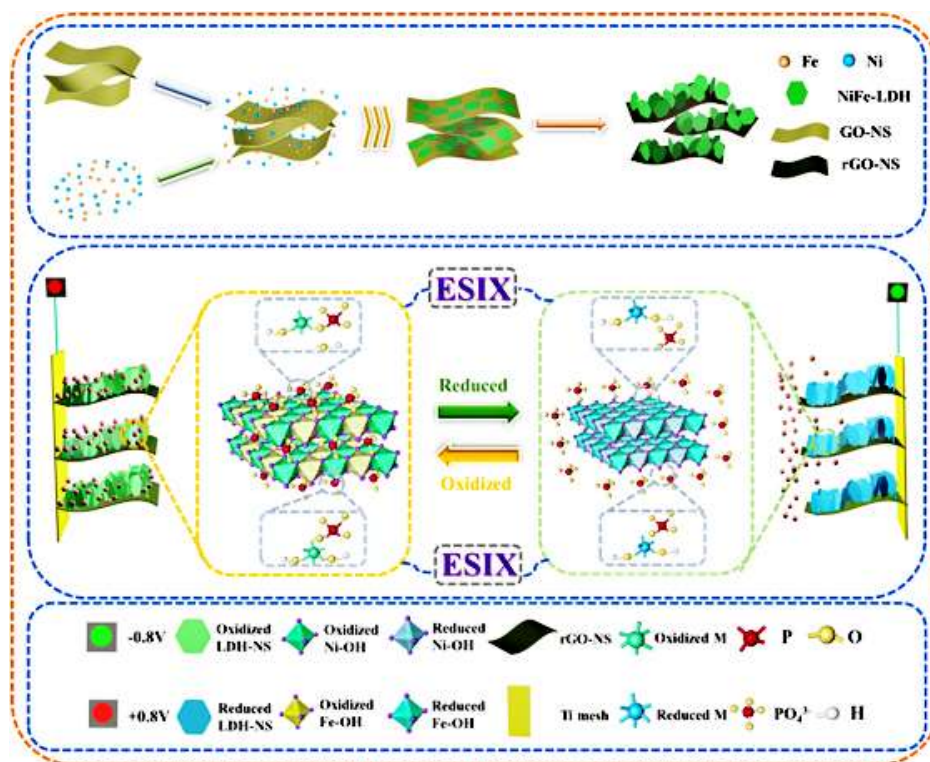
206

207 Scheme.1. Schematic illustration for the preparation process of the NiFe-LDH/rGO hybrid

208 film and its uptake/release mechanism for phosphate anions

209 **3.1 Microstructure and elements distribution**

3.1.1 SEM analyses
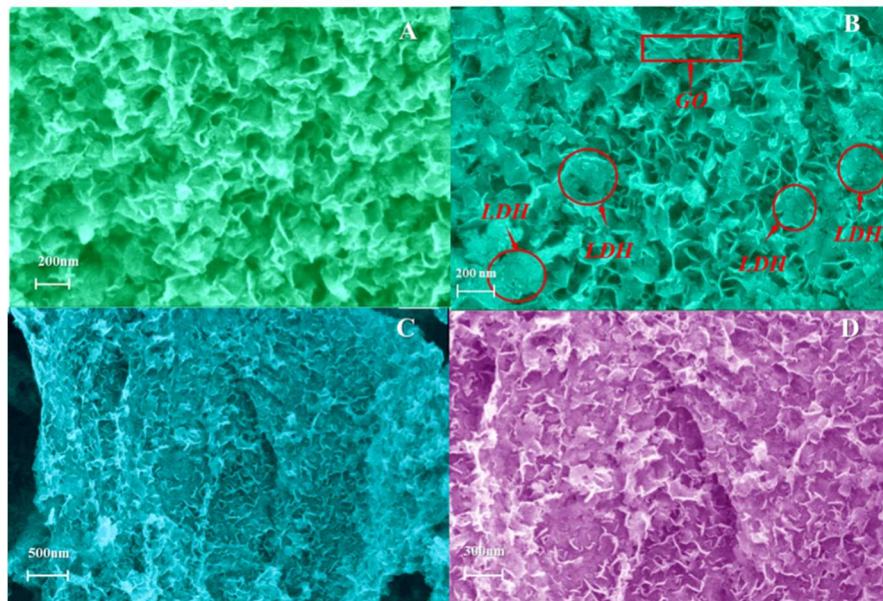
Fig.1. (A, B) SEM images of NiFe- LDH and NiFe- LDH/GO hybrid matrials; (C, D) SEM image

of NiFe-LDH/rGO hybrid matrials at different magnification (500nm and 200nm)

Fig.1 shows the SEM of the microscopic morphology of the materials. As shown

in Fig.1 A, the pure NiFe-LDH material prepared by hydrothermal method presents a

regular two-dimensional nanosheet structure with uniform dispersion and a size range

of about 50 nm to 300 nm, which is relatively small compared with other LDH materials,

such as CoAl-LDH (Forticaux et al., 2015), MgAl-LDH (Ghani et al., 2018) and ZnAl-

LDH (He et al., 2010). The advantage of this phenomenon is that small size LDH tablets

have a less hindering effect on ion implantation and removal than large size LDH tablets.

Fig.1 B shows the NiFe- LDH/GO hybrid material was successfully prepared, and the

NiFe-LDH nanosheets were tiled on the surface of GO lamella. As shown in Fig.1 C-

D, the NiFe-LDH nanosheets grow on the surface of rGO lamella at different angles

and are evenly dispersed after further reduction by hydrazine hydrate steam. Compared

with the NiFe-LDH/GO hybrid material, the NiFe-LDH/rGO provides more favorable

226   conditions for the uptake and release of phosphate anions, and the rGO further improves

227   the conductivity of the hybrid material and reduces the resistance of electron transfer in

228   the electrochemical redox process.

229   **3.1.2 Analyses of XRD and FT-IR**
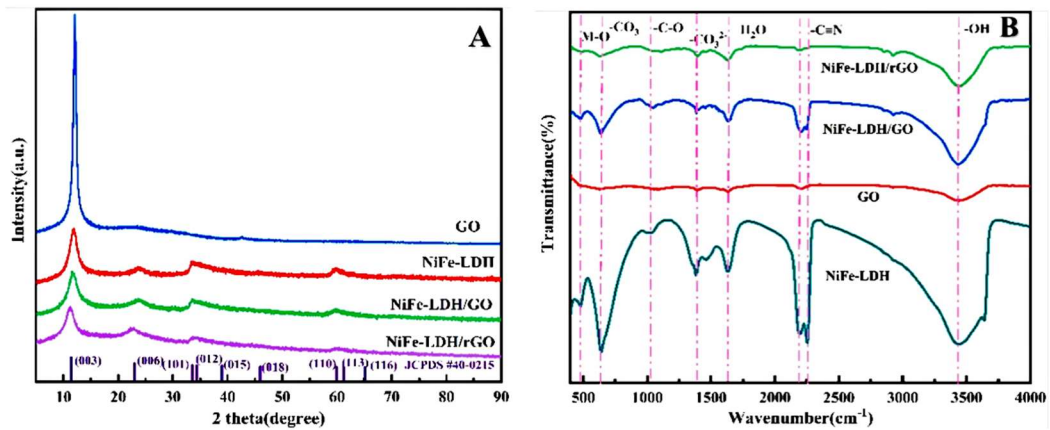
230

231   Fig.2. XRD patterns(A) and FT-IR(B) spectra of GO, NiFe-LDH, NiFe-LDH/GO and NiFe-

232   LDH/rGO hybrid matrials

233   To verify the recombination of the materials, the XRD and FT-IR were performed.

234   As shown in Fig.2 A, the NiFe-LDH material containing carbonate intercalation was

235   successfully prepared, which was confirmed by the identical peak at 11.42°, 23.63°,

236   33.74° and 60.12°, corresponding to (003), (006), (012) and (110) faces of

237    $Ni_{0.75}Fe_{0.25}(CO_3)_{0.125}(OH)_2 \cdot 0.38H_2O$ (JCPDS #40-0215). Compared with the pure

238   NiFe-LDH, the NiFe-LDH/GO and NiFe-LDH/rGO exhibited similar four main peaks,

239   indicating that the addition of GO did not affect the crystal structure of NiFe-LDH (Abo

240   et al., 2020) even during the reduction process. Quite interestingly, the intensity of

241   diffraction peaks at about 12° decrease and gradually shift left after introduction of GO

242   and subsequent reduction process, suggesting that the change of surface or interface

243 between GO/rGO occurred and LDH has grown on it. This effect was beneficial to

244 further prove the success of the composite of the two materials.

245   Furthermore, the FT-IR of the NiFe-LDH/rGO composite materials were analyzed

246 in Fig. 2 B. It can be seen that the wide peak at 3436 cm^{-1} is attributed to the stretching

247 vibration of -OH bond. The peak at 1375 cm^{-1} and 642 cm^{-1} proved the generation of

248 carbonate anions between LDH layers (Zhao et al., 2018). The peak at 468 cm^{-1} was

249 caused by the stretching vibration of M-O bond. The appearance of the above peak

250 pattern further proves that the NiFe-LDH material had been successfully prepared (Cao

251 et al., 2019).

252   As shown in Fig. 2 B, the peaks of pure GO corresponding at 1096 cm^{-1}, 1397 cm^{-1}

253 1628 cm^{-1}, 2202 cm^{-1} and 3436 cm^{-1} (Tian et al., 2019). Although the characteristic

254 absorption peak of the NiFe-LDH/GO hybrid material weakened after binding with GO,

255 the position of the peak emergence did not change significantly. In addition, the

256 stretching peak and bending peak of the M-O bond of the NiFe-LDH /GO hybrid

257 material were consistent with that of the NiFe-LDH. Thus, it was proved that the NiFe-

258 LDH successfully loads on the GO surface. After reduction by hydrazine hydrate steam,

259 it can be seen from Fig.2 B that the characteristic absorption peaks of NiFe -LDH did

260 not disappear, but the intensity of absorption peaks was significantly weakened,

261 indicating that after reduction by hydrazine vapor, a large number of oxygen-containing

262 functional groups of the hybrid material were reduced, which was the reduction process

from GO to rGO. It indicates that the NiFe-LDH/rGO hybrid material was successfully

prepared, which were consistent with the XRD and SEM results.
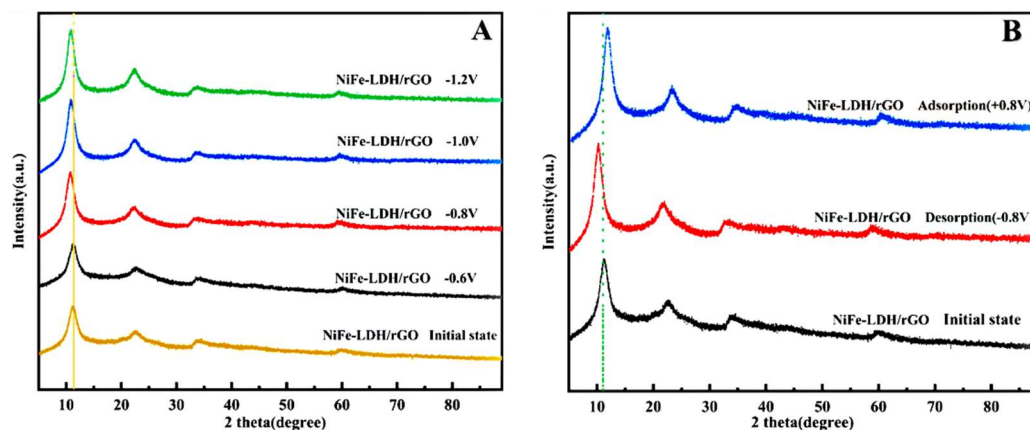
Fig.3. XRD patterns of NiFe-LDH/rGO hybrid film (A) desorption (0.1M $NaNO_3$ electrolyte

solution) at the different voltages (-0.6, -0.8, -1 and -1.2 V); (B) desorption (0.1M $NaNO_3$

electrolyte solution) and adsorption (0.1M Na_3PO_4 electrolyte solution) at ±0.8 V

Fig.3 shows the XRD patterns of the desorption and adsorption of the NiFe-

LDH/rGO hybrid film at different voltages and the desorption/adsorption at 0.8 V. In

the process of preparing LDH, urea was used to provide an alkaline environment, and

urea will be decomposed to produce CO_2 when heated, resulting in a certain amount of

carbonate intercalated anions in the prepared NiFe-LDH/rGO hybrid film. In terms of

the theoretical selectivity of LDH to each anions, $PO_4^{3-} > CO_3^{2-} > SO_4^{2-} > OH^- > F^- >$

$Cl^- > NO_3^-$, carbonate anions have a great influence on the adsorption effect of

phosphate anions (Zhao et al., 2020; He et al., 2018). Therefore, the electrochemical

method is adopted to remove the intercalated carbonate anions in the hybrid film as far

as possible. It is particularly important to convert it to other anions with less impact,

such as nitrate anions.

280   As can be seen from Fig. 3 A, in 0.1 M sodium nitrate solution, the peak height

281   corresponding to the (003) position changes significantly under different desorption

282   voltages. When the desorption voltage reaches -0.8 V, the peak corresponding to the

283   (003) position shifts slightly to the left, indicating that the laminar spacing of LDH has

284   expanded. Carbonate anions were released into the solution rich in nitrate anions

285   because of the gradient od concentration.When the power was disconnected

286   instantaneously, part of nitrate anions was transferred into the LDH between layer board.

287   Although there was a small shift at -1 and -1.2 V, the electroactive film swelling

288   phenomenon happened at -1.0 V, when the voltage was -1.2 V the electroactive film

289   and conductive matrix will be separated as they were not conducive to the subsequent

290   placement and removal of phosphate anions. Therefore, the pre-desorption voltage was

291   chosen as -0.8 V.

292   After the desorption at -0.8 V, the adsorption of phosphate anions was investigated

293   at 0.8 V. As can be seen from Fig.3 B, compared to the NiFe-LDH/rGO, the main peak

294   of the desorption sample shifted to the left, which was caused by the increase of laminar

295   spacing of LDH caused by nitrate anions implantation. Afterward, electrochemical

296   adsorption of phosphate anions was carried out at 0.8 V oxidation potential in 0.1M

297   sodium phosphate solution, and it could be easily found that the corresponding peak at

298   (003) of the adsorption sample shifted to the right. This evidence indicates that the

299   laminar spacing of LDH decreased because of the replacement of nitrate anions with

300   phosphate anions. In this work, The change of LDH layer spacing caused by the

301   addition of phosphate anions and nitrate anions is mainly caused by two aspects. On

the one hand, the binding mode of LDH to nitrate anions mainly depends on the surface

complexation of physical properties, but the binding mode of LDH to phosphate anions

is mainly the formation of inner sphere complexation with strong chemical effects.

Metal Fe/Ni provides a specific adsorption site to achieve the adsorption of phosphate

anions, which can also be explained by XPS spectra; On the other hand, due to the

affinity between LDH and oxygen-containing acid anions (especially phosphate anions)

are superior to other anions, the LDH spacing will show a slightly decreasing trend

(Zhao et al., 2017). This situation shows that in electrolyte solutions of different systems,

the change of interlayer spacing is not only related to the diameter of anions in solution

but also is the result of the combined action of the diameter of anions in solution,

valence state, surface physicochemical reaction and binding energy of each anion by

LDH (Morimoto et al., 2012).

3.1.3 Electrochemical test
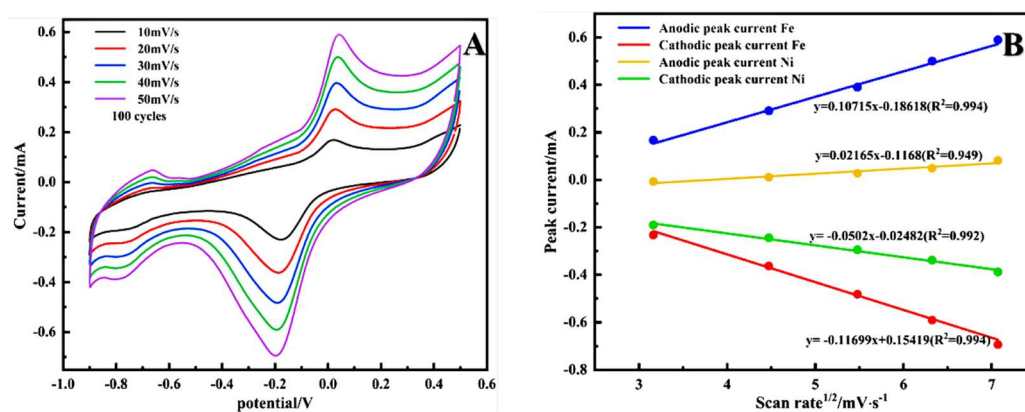
Fig .4. (A) CV curves of NiFe-LDH/rGO hybrid films in 0.1M Na_3PO_4 solution at 10, 20, 30, 40,

50 mV/s, respectively; (B) The variation of anode and cathode peak current of the NiFe-LDH

/rGO hybrid film with the square root of scanning speed in 0.1 M Na_3PO_4 solution

319   The rate control steps of the NiFe-LDH/rGO hybrid film on phosphate anions were

320   analyzed through the cyclic voltammetry curve. Fig. 4 shows the CV curve of the hybrid

321   film at different scanning rates in 0.1M Na_3PO_4 solution, as well as the variation of the

322   anodic and cathodic peak currents with the scanning rate. Theoretically, the relationship

323   between peak current and sweep speed at different sweep speeds should satisfy the

324   following equation:

325
$$i = av^b$$

326   In which, i refers to the peak current (mA)at a specific sweep speed; v indicates

327   the scanning rate, in mV/s. a and b indicate related parameters. In general, when

328   parameter b =1, it represents the process of capacitive diffusion control; When b=0.5,

329   it represents a semi-infinite diffusion controlled process, that is, there is an simply redox

330   reaction (Chen et al., 2018). As shown in Fig. 4 A, two pairs of symmetrical redox peaks

331   can be observed in any of the CV curves, which exactly correspond to the valence

332   changes of nickel and iron elements, indicating that the electrochemical reaction

333   process of the NiFe-LDH/rGO hybrid film on phosphate anions is reversible (Yang et

334   al., 2021). With the increase of sweep speed, the electric capacity gradually increases,

335   showing good electrochemical performance. It can be seen from Fig. 4 B that the square

336   root of peak anodic and cathodic currents with sweep velocity present a linear

337   correlation coefficient greater than 0.95, which further indicates that the

338   electrochemical reaction process of the hybrid film on phosphate anions is reversible.

339   It further indicates that the electrochemical reaction of NiFe-LDH/rGO hybrid film to

340   phosphate anions is a semi-infinite diffusion controlled process (Hao et al., 2012).

3.1.4 XPS characterization
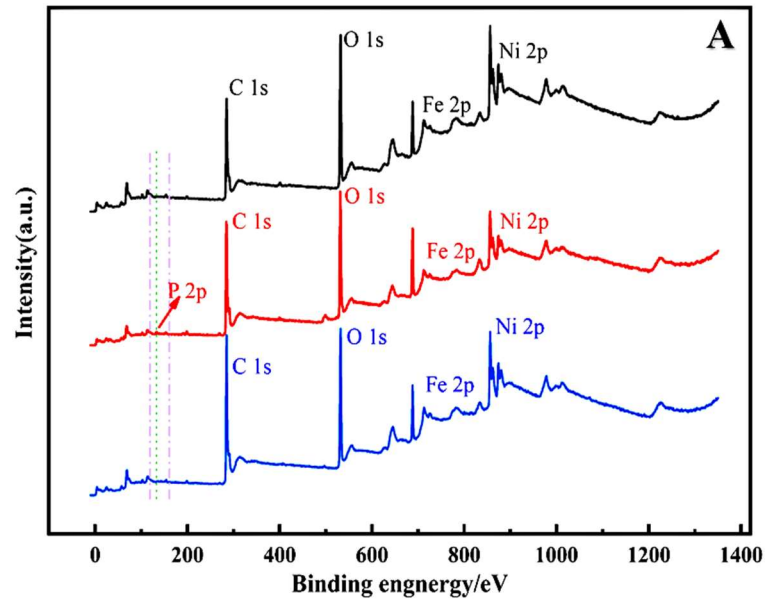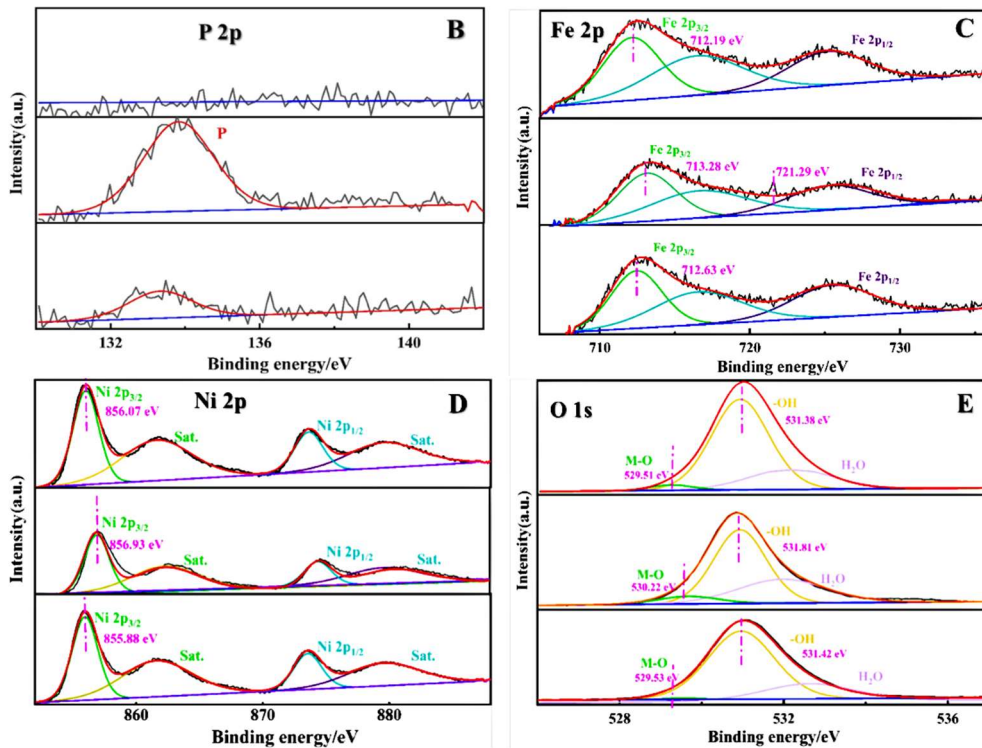
345   Fig.5. XPS spectra of NiFe-LDH/rGO hybrid films in 0.1M Na_3PO_4 solution at initial (top),

346   oxidation (middle) and reduction (bottom) states: (A) full spectrum, (B)P 2p, (C) Fe 2p, (D) Ni 2p

347   and (E) O 1s

348

349   In order to further clarify the mechanism of electrochemical implantation and

350   removal of phosphate anions by NiFe-LDH/rGO hybrid film, the film were

351   characterized by XPS in the initial state, oxidation state and reduction state. As can be

352   seen from Fig.5 A, the existence of elements such as Ni, Fe, O and P proves that the

353   film has been successfully prepared.In addition, it can be seen from Fig.5 B that in the

354   oxidation state, there is an obvious P peak at 133.85 eV, which proves that P is inserted

355   into the hybrid film, while in the reduction state, there is basically no P peak, which

356   also illustrates that P is successfully removed from the film. These results indicate that

357   the implantation and removal of phosphate anions by the NiFe-LDH/rGO hybrid film

358   are reversible.

359   In the electrochemical redox process,the transformation of the electroactive film

360   in the redox process is the premise for the successful placement and removal of

361   phosphate anions in the hybrid film, which is also the unique advantage of ESIX. Fig.5

362   C and D respectively explore the XPS spectra of Fe 2p and Ni 2p in the initial oxidation

363   and reduction states. As can be seen from Fig.5 C and Table S1, compared to the initial

364   state, the peak distribution of Fe $2p_{1/2}$ and Fe $2p_{3/2}$ decreased significantly at the

365   oxidation potential state, namely the adsorption of phosphate anions. More in detail,

366   the peak area ratio at Fe $2p_{3/2}$ decreased from 36.29% to 33.96%. Moreover, as the

367   binding energy of Fe $2p_{3/2}$ increases from 712.19 eV to 713.28 eV. These phenomena

368   occur because under the influence of reduction potential, the atom loses part of its

369   charge, the shielding effect of outer electrons on inner electrons weakens, and the

370   density of electron cloud decreases, leading to the possibility that part of Fe may change

371   from +2 valence to +3 valence. To compensate for the loss of interlayer charge,

372   phosphate anions will be placed between LDH layers (Youmbi et al., 2021). When the

373   hybrid film was in the reduction potential state, that is, desorption of phosphate anions,

374   the peak area ratio and peak distribution of Fe 2p increased significantly, and the peak

375   area ratio at Fe $2p_{3/2}$ increased from 33.96% to 37.16%. Meanwhile, the binding energy

376   at Fe $2p_{3/2}$ decreased from 713.28 eV to 712.64 eV. Compared with the phenomenon in

377   the electrochemical oxidation state, in the electrochemical reduction state, atoms gain

378   partial charge, the shielding effect of external electrons on internal electrons is

379   enhanced, and the density of electron cloud increased. It indicates that part of Fe^{3+} turns

380   into Fe^{2+}, thus improving the electronegativity of the hybrid film. In order to balance

381   the excess phosphate anions between layers, the phosphate anions will be removed from

382   the film. In addition, in Fig.5 C, there is a clear peak at 721.29 eV in the oxidation state,

383   indicating that the binding of Fe and P is in the form of Fe-O-P bond (Wan et al., 2020).

384   As can be seen from Fig.5 D and Table S1, compared to the initial state, in the

385   electrochemical oxidation state, the peak area ratio at Ni $2p_{3/2}$ decreased from 29.39%

386   to 25.52%, and the peak distribution of Ni $2p_{1/2}$ and Ni $2p_{3/2}$ also decreased significantly.

387   The binding energy of Ni $2p_{3/2}$ increased from 856.07 eV to 856.93 eV. It also indicates

388   that the atom loses part of its charge, and the density of the electron cloud decreases,

389   leading to the possibility that some Ni valence may change from +2 to +3. To integrate

390   the loss of interlayer charge, phosphate anions are placed between LDH layers. These

391   indicate that the combination of Ni and P is similar to that of Fe, in the form of Ni-O-P

392   bond (He et al., 2018). Similarly, when the hybrid film was in the reduction state, the

393   peak area ratio and peak distribution of Ni 2p increased significantly, and the peak area

394   ratio at Ni $2p_{3/2}$ increased from 25.52% to 30.45%. Meanwhile, the binding energy at

395   Ni $2p_{3/2}$ also decreased from 856.93 eV to 855.88 eV. It indicates that part of Ni^{3+}

396   changes into Ni^{2+}, which improves the electronegativity of the hybrid film and makes

397   phosphate anions separated from the film. However, in the electrochemical redox state,

398   the peak positions of nickel and iron ions in the reduced state cannot coincide with the

399   peak positions in the initial state, and a slight deviation occurs. Analyzes its reason, and

400   it could be in the initial state, LDH layers contain part of carbonate anions, while

401   stripping the electrolyte of sodium nitrate solution, in part to take off the attached LDH

402   layers containing nitrate anions (Zhao et al., 2018). The binding energies of nitrate,

403   carbonate and phosphate are different between LDH layers, leading to the failure to

404   coincide with the initial peak after reduction. This phenomenon can be mutually

405   confirmed with the XRD analyses mentioned above.

406   Although the above situation systematically explains the mechanism of the

407   placement and removal of phosphate anions from the hybrid film, the specific

408   combination between the hybrid film and phosphate remains to be further discussed. In

409   order to further verify the bonding mode between Ni/Fe metal (replaced by M) and P,

410   the change form of O before and after oxidation was tested. As can be seen from Fig.5

411   E, the peak distribution of M-O increased significantly in the oxidation state. It can be

412   seen from Table S1 that the peak area ratio of M-O increases from 3.24% to 9.41%,

413   while the peak area ratio of -OH decreases from 67.52% to 55.38%. This phenomenon

414   indicates that hydroxyl groups on the surface of the conductive hybrid film are involved

415   in the adsorption of phosphate anions, resulting in the replacement of hydroxyl groups

416   by phosphate anions. It is indirectly explained that the binding mode of nickel-iron

417   bimetal and phosphate ion is M-O-P in the form of intramolecular complexation

418   (Morimoto et al., 2012). When the conductive hybrid film is in the reduction state, the

419   peak area ratio of M-O decreases from 9.41% to 0.95%, and on the contrary, the -OH

420   increases from 55.38% to 68.77%, indicating that the -OH peak is reconstituted and the

421   phosphoric acid escapes into the system to be received (Rahman et al., 2021). This

422   illustrates in detail to some extent that at the oxidation potential, the binding mode of

423   NiFe-LDH/rGO hybrid film to phosphate anions exists in the form of M-O-P.

424   **3.2 Adsorption performance test**
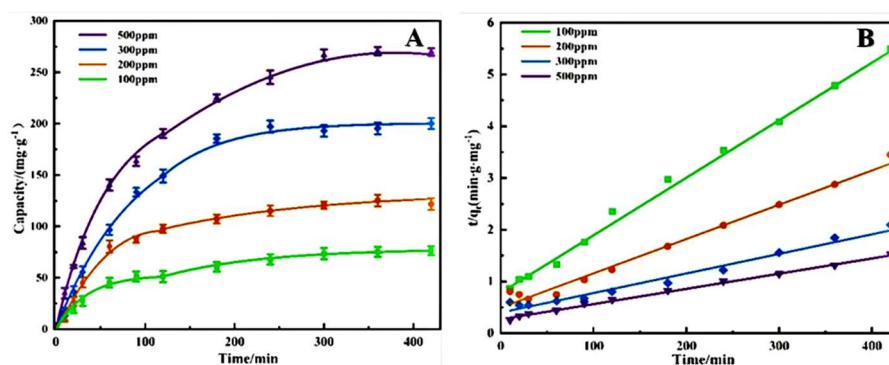
Fig.6. (A) adsorption capacity of NiFe-LDH/rGO hybrid films for phosphate anions at different

initial concentrations;(B) pseudo-second-order adsorption kinetics curves of NiFe-LDH/rGO

hybrid films for phosphate anions at different initial concentrations.
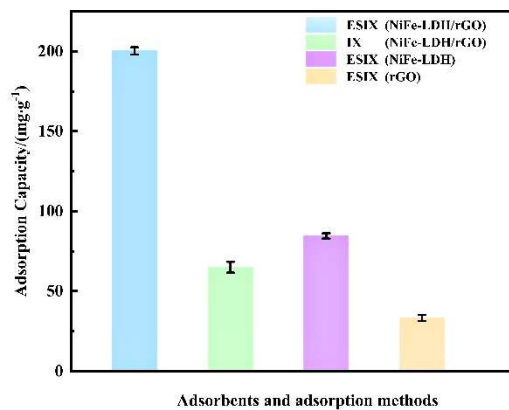
430

431   Fig. 7. Phosphate anions uptake capacity curves of ESIX (NiFe-LDH/rGO), IX (NiFe-LDH/rGO),

432   ESIX (NiFe-LDH) and ESIX (rGO)

433   Fig.6 shows the adsorption capacity diagram and pseudo-second-order adsorption

434 kinetics curve of the NiFe-LDH/rGO hybrid film for phosphate anions in 17mL solution

435 at different initial concentrations. As can be seen from Fig.6 A, the hybrid film has a

436 high adsorption capacity for phosphate anions, and it increases with the initial

437 concentration. When the initial concentration is 500 ppm, the film's adsorption capacity

438 for phosphate anions can reach about 270 mg·g^{-1}. Compared with Table S3, the film

439 has a better adsorption capacity for phosphate anions. In addition, Fig.6 B analyzes the

440 adsorption kinetics of the film through pseudo-first-kinetic models and second-order

441 kinetic models, to understand the reaction rate control steps of the film to phosphate

442 anions. The establishment of pseudo-first-order dynamics model (Eq. (4)) and pseudo-

443 second-order dynamics model (Eq. (5)) are analyzed by the following equation (Ji et

444 al., 2022).

445
$$ln(q_e - q_t) = lnq_e + k_1t \tag{4}$$

446
$$\frac{t}{q_t} = \frac{t}{q_e} + \frac{1}{k_2 q_e^2} \tag{5}$$

447   K_1 is a pseudo-first-order kinetic parameter, and the unit is min^{-1}. q_e and q_t are

448   respectively the adsorption capacity of the hybrid film on phosphate anions when the

449   adsorption reaches equilibrium and the adsorption capacity at time t (min), in mg·g^{-1}.

450   K_2 is a pseudo-second-order kinetic parameter, and the unit is g·mg^{-1}·min^{-1}. Table S2

451   shows the relevant parameters of pseudo-first-order and second-order dynamics models

452   obtained through the fitting. As can be seen from Fig.6 B and Table S2, compared with

453   the pseudo-first-order kinetic curve, the pseudo-second-order kinetic curve has a higher

454   correlation coefficient (R^2), indicating that the rate-limiting step of the electrochemical

455   adsorption process of phosphate anions are dominated by chemisorption (Ji et al., 2022).

456   To investigate the actual efficiency of NiFe-LDH/rGO hybrid film on phosphate

457   anions, different adsorption films and charging methods were used in Fig.7 to explore

458   the adsorption capacity of phosphate anions. As can be seen from Fig.7, after 6 h of

459   adsorption, the adsorption capacity of hybrid film film for phosphate anions only

460   reaches 65.2 mg·g^{-1} by IX technology, which is about 1/3 of that by IX technology and

461   far lower than that by ESIX technology. Under the action of 0.8 V, the adsorption

462   capacity of LDH and rGO is 84.52 and 33.33 mg·g^{-1}, respectively, which is much lower

463   than that of NiFe-LDH and rGO doping. The results show that the incorporation of rGO

464   can significantly improve the electrochemical redox characteristics of NiFe-LDH, and

465   further improve the adsorption capacity of anions. The reasons for the high adsorption

466   capacity of NiFe-LDH/rGO hybrid film for phosphate anions may be: (1) the pushing

467   diffusion force of ions: IX technology only adsorbs phosphate anions in the way of

468   concentration difference, but ESIX technology is the result of concentration difference

469 and potential difference; (2) ESIX technology changed the redox potential of the film,

470 resulting in the change of the valence state of nickel-iron ion between the laminates,

471 resulting in the increase of the adsorption capacity of phosphate anions on the hybrid

472 film. However, the simple LDH did not find such a situation, which may be because

473 ESIX technology is the result of the interaction between ions and electrons, so the

474 simple LDH only provides ion transport channels, without causing electron transport

475 and valence state transformation. Similarly, rGO could provide only electronic

476 transmission channels.
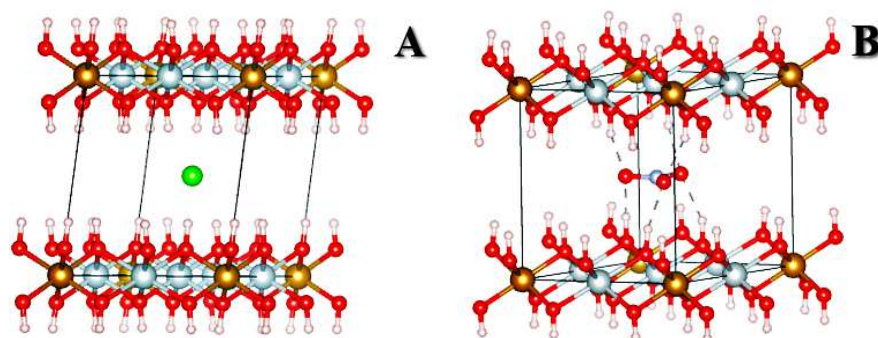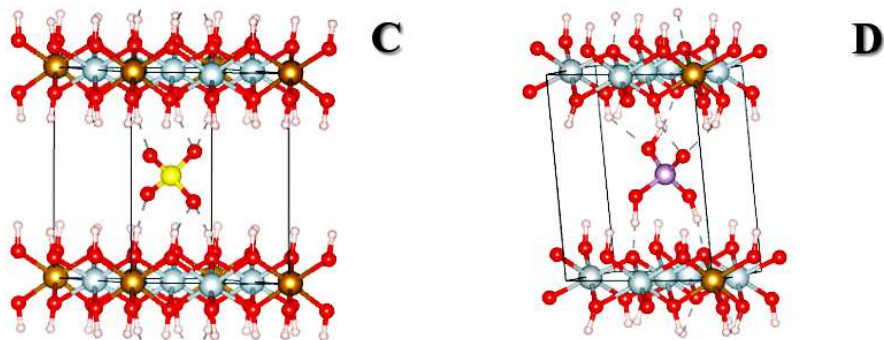
477 **3.2.2 Adsorption selectivity**
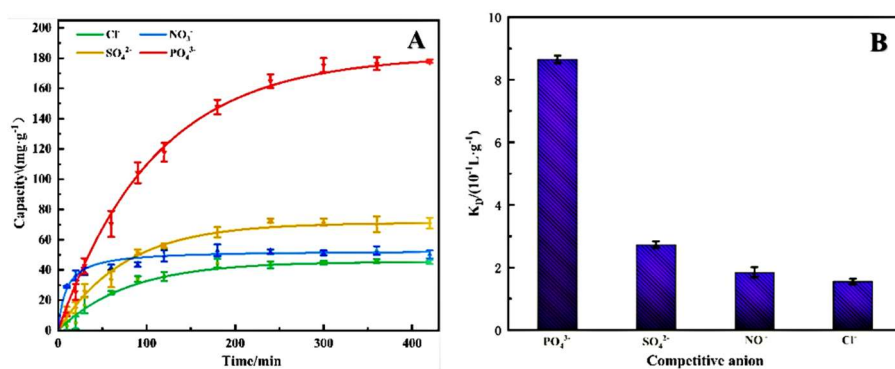
479 Fig.8. (A) competitive adsorption curve and (B) separation coefficient of PO_4^{3-}, SO_4^{2-}, NO_3^- and

480 Cl^- for NiFe-LDH/rGO hybrid films at an initial concentration of 300 ppm

481

Fig.9. The calculated binding energies of NiFe-LDH/rGO hybrid films for (A) chloride , (B) nitrate , (C) sulfate and (D) phosphate anions

In order to determine the adsorption selectivity of phosphate anions on the hybrid film of NiFe-LDH /rGO, the competitive adsorption of phosphate anions on the hybrid film was determined by competitive adsorption in the mixed solution of sodium phosphate, sodium sulfate, sodium nitrate and sodium chloride at the concentration ratio of 1:1:1:1. Fig.8 shows competitive adsorption curves and separation coefficients of PO_4^{3-}, SO_4^{2-}, NO_3^- and Cl^- on the hybrid film of NiFe -LDH/rGO at a volume of 17mL and an initial concentration of 300 ppm. As can be seen from Fig.8 A, although the NiFe-LDH/rGO hybrid film has certain adsorption performance for PO_4^{3-}, SO_4^{2-}, NO_3^- and Cl^-, its adsorption performance for phosphate anions is significantly superior to other anions, proving that the film has excellent adsorption selectivity for phosphate anions.

Moreover, to further clarify the excellent specific selective adsorption of phosphate anions by NiFe -LDH/rGO hybrid film, the selective adsorption of PO_4^{3-}, SO_4^{2-}, NO_3^- and Cl^- by the hybrid film was explored by electrochemical CV. In order to keep the anionic charges uniform, the solution is 0.3M $NaNO_3$, 0.3M NaCl, 0.15M $NaSO_4$ and 0.1M Na_3PO_4 electrolytic solutions, respectively. As can be seen from Fig.

S1, the CV curves of the hybrid film film for SO_4^{2-}, NO_3^- and Cl^- are controlled by double electric layers, and there is no redox process. However, it shows pseudocapacitance control for phosphate anions, that is to say, these competing anions are only physically attached to the surface of the film, unlike phosphate anions. This is the best explanation for the apparent superior selectivity of phosphate anions over other competing anions.

Fig.8 B shows the separation coefficients of several anions by the NiFe-LDH/rGO hybrid film. Combining (Eq. (2)) and Table S4, it can be obtained that the separation coefficients of PO_4^{3-}, SO_4^{2-}, NO_3^- and Cl^- by the hybrid film are 0.86, 0.27, 0.18 and 0.16, respectively. This indicates that the film has excellent adsorption selectivity for phosphate anions. Meanwhile, according to the calculation results of (Eq. (4)), it can be seen from Table S4 that in terms of relative separation factors, the relative separation factors of PO_4^{3-}/SO_4^{2-}, PO_4^{3-}/ NO_3^- and PO_4^{3-}/ Cl^- are 3.16, 4.68 and 5.55, respectively. This further indicates that the NiFe-LDH/rGO hybrid film has a very good adsorption selectivity for phosphate anions. The reason may be that phosphate anions are valence anions of -3, which have a higher valence state than other anions. In terms of pure electrostatic interaction, negatively charged phosphate anions can adhere to the surface and interlayer of the positively charged NiFe-LDH bimetal laminate faster. Secondly, compared with the surface complexation of other anions, the NiFe-LDH bimetal laminates and phosphate anions bind in a stronger way of intracellular complexation (Morimoto et al., 2012).

523   Furthermore, in order to explore the reason why NiFe-LDH shows excellent

524   selection performance for phosphate anions, AMS software is used to conduct DFT

525   calculation for the NiFe-LDH in Fig.9 to explore their binding energy for chloride,

526   nitrate, sulfate and phosphate anions. The results show that the binding energies of the

527   NiFe-LDH for phosphate, sulfate, nitrate and chloride anions are -657.576, -565.573, -

528   352.932 and -381.223 kJ·mol^{-1} in Table S5 and S6, respectively. The binding energies

529   for phosphate anions are significantly more negative than other anions. The NiFe-LDH

530   show stronger binding force to phosphate anions. It can be seen from the side that under

531   the same conditions, NiFe-LDH preferentially binds phosphate anions. This further

532   explains that the selective recognition ability of NiFe-LDH for phosphate anions is

533   higher than that of the other anions.

534   **3.2.3 Stability test**
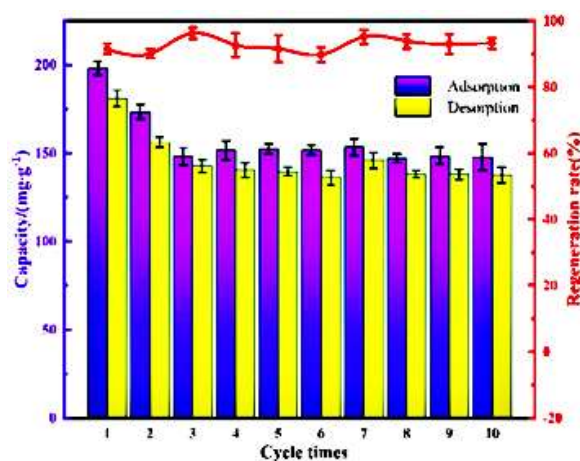
535

536   Fig.10. The adsorption and desorption capacity of NiFe-LDH/rGO hybrid film for phosphate

537   anions in 300 ppm sodium phosphate and sodium nitrate solutions, respectively

538   Furthermore, the reduction equipment and operating cost, and the increasing of the

539   working time are key objectives of modern industries (Velusamy et al., 2021). For this

540   reasons, in the work herein the reciclability of the film was investigated. Fig.10   shows

the adsorption/desorption capacity and regeneration efficiency curve of the NiFe-LDH /rGO hybrid film for phosphate anions within 10 cycles. As can be seen from the Fig. 10, after about 3 cycles, the placement and removal of phosphate anions by the NiFe-LDH /rGO hybrid film basically stabilized, and the regeneration efficiency remained above about 85%, showing good cycle stability, which provided a possibility for the industrial application of the film to absorb phosphate anions in the future. In the first three cycles, the adsorption capacity of the film for phosphate anions decreases. On the one hand, it may be because some phosphate anions and the NiFe-LDH bimetal laminates have strong intracellularly complexation, which results in some phosphate anions not being separated from the NiFe-LDH bimetal laminates. On the other hand, the adsorption capacity of phosphate anions decreases in the first three cycles, possibly because part of phosphate anions are placed between bimetallic laminates, which balances the charge between the laminates. But in general, the hybrid film shows excellent cyclic stability for phosphate anions. Such good cyclic stability is also reflected in Fig. S1, indicating that the hybrid film has excellent redox properties for phosphate anions, and the uptake and release of phosphate anions are reversible, which effectively avoids the generation of secondary pollution. In addition. The stability of the hybrid film in acid and alkaline solutions is investigated in Fig.S2. It can be seen that the hybrid film can stably exist in neutral and alkaline solutions, which provides a certain reference for the separation of phosphate anions in neutral and alkaline wastewater.

4 Conclusion

In summary, this study successfully prepared a kind of the NiFe-LDH/rGO hybrid film with high selectivity for phosphate anions. Compared with LDH alone, the addition of rGO further improves the conductivity of the film, which has a good promotion effect on improving the electrochemical performance of the film. At a voltage of 0.8 V, the adsorption capacity of the hybrid film film for phosphate anions is as high as 270 mg·g^{-1}, which is much higher than that reported in other literature, mainly due to the synergistic driving force caused by electrochemical redox. At the same time, the hybrid film also shows high selectivity to phosphate anions in the presence of various competing anions. In addition, after 10 cycles, the regeneration efficiency of the hybrid film film is above 85%, with good cycle stability and excellent desorption performance. Although the adsorption capacity of the film to phosphate anions decreases under acidic conditions, it can exist stably in neutral and alkaline solutions, which has a good reference for the removal of phosphate anions in industrial medium and alkaline solutions.

Declaration of Competing Interest

There are no conflicts to declare.

Acknowledgement

607 [1]Velusamy K, Periyasamy S, Kumar P S, Vo D-V N, Sindhu J, Sneka D, Subhashini B. Advanced

608 techniques to remove phosphates and nitrates from waters: a review. Environmental Chemistry

609 Letters, 2021, 19(4): 3165-80. doi: 10.1016/j.jhazmat.2014.10.048.

610 [2]Sun Y, Feng X, Zheng W. Nanoscale lanthanum carbonate hybridized with polyacrylic resin for

611 enhanced phosphate removal from secondary effluent. Journal of Chemical & Engineering Data,

612 2020, 65(9): 4512-22. doi: 10.1021/acs.jced.0c00352.

613 [3]Wu B, Lo I M C. Surface Functional group engineering of CeO_2 particles for enhanced phosphate

614 adsorption. Environ Sci Technol, 2020, 54(7): 4601-8. doi: 10.1021/acs.est.9b06812.

615 [4]Wu B, Wan J, Zhang Y, Pan B, Lo I M C. Selective phosphate removal from water and wastewater

616 using sorption: process fundamentals and removal mechanisms. Environ Sci Technol, 2020, 54(1):

617 50-66. doi: 10.1021/acs.est.9b05569.

618 [5]Hassan M H, Stanton R, Secora J, Trivedi D J, Andreescu S. Ultrafast removal of phosphate from

619 eutrophic waters using a cerium-based metal-organic framework. ACS Appl Mater Interfaces, 2020,

620 12(47): 52788-96. doi: 10.1021/acsami.0c16477.

621 [6]Zou H, Wang Y. Phosphorus removal and recovery from domestic wastewater in a novel process

622 of enhanced biological phosphorus removal coupled with crystallization. Bioresour Technol, 2016,

623 211: 87-92. doi: 10.1016/j.biortech.2016.03.073.

624 [7]Wu B, Fang L, Fortner J D, Guan X, Lo I M C. Highly efficient and selective phosphate removal

625 from wastewater by magnetically recoverable $La(OH)_3/Fe_3O_4$ nanocomposites. Water Res, 2017,

626 126: 179-88. doi: 10.1016/j.watres.2017.09.034.

627 [8] Gu B , Brown G M , Chiang C C . Treatment of perchlorate-contaminated groundwater using

628 highly selective, regenerable ion-exchange technologies. Environmental Science & Technology,

2007, 41(17):6277. doi: 10.1021/es0706910.

[9]Yang Y, Du X, An X, Ding S, Liu F, Zhang Z, Ma X, Hao X, Guan G, Zhang H. Potential-induced reversible uptake/release of perchlorate from wastewater by polypyrrole@CoNi-layered double hydroxide modified electrode with proton-ligand effect. J Colloid Interface Sci, 2018, 523: 159-68. doi: 10.1016/j.jcis.2018.03.098.

[10]Morimoto K, Anraku S, Hoshino J, Yoneda T, Sato T. Surface complexation reactions of inorganic anions on hydrotalcite-like compounds. J Colloid Interface Sci, 2012, 384(1): 99-104. doi: 10.1016/j.jcis.2012.06.072.

[11]Nuryadin A, Imai T, Kanno A, Yamamoto K, Sekine M, Higuchi T. Phosphate adsorption and desorption on two-stage synthesized amorphous-ZrO_2/Mg–Fe layered double hydroxide composite. Materials Chemistry and Physics, 2021, 266:124559. doi: 10.1016/j.matchemphys.2021.124559.

[12]Liu C, Zhang M, Pan G, Lundehøj L, Nielsen U G, Shi Y, Hansen H C B. Phosphate capture by ultrathin MgAl layered double hydroxide nanoparticles. Applied Clay Science, 2019, 177: 82-90. doi: 10.1016/j.clay.2019.04.019.

[13]Hong S P, Yoon H, Lee J, Kim C, Kim S, Lee J, Lee C, Yoon J. Selective phosphate removal using layered double hydroxide/reduced graphene oxide (LDH/rGO) composite electrode in capacitive deionization. J Colloid Interface Sci, 2020, 564: 1-7. doi: 10.1016/j.jcis.2019.12.068.

[14]Rahman S, Navarathna C M, Krishna Das N, Alchouron J, Reneau P, Stokes S, R V K G T, Perez F, Barbary Hassan E, Mohan D, Pittman C U, Jr., Mlsna T. High capacity aqueous phosphate reclamation using Fe/Mg-layered double hydroxide (LDH) dispersed on biochar. Journal of Colloid and Interface Science, 2021, 597: 182-95. doi: 10.1016/j.jcis.2021.03.114.

[15]Niu J, Yan W, Du J, Hao X, Wang F, Wang Z, Guan G. An electrically switched ion exchange

651 film with molecular coupling synergistically-driven ability for recovery of Ag^+ ions from

652 wastewater. Chemical Engineering Journal, 2020, 389:124498. doi: 10.1016/j.cej.2020.124498.

653 [16]Du X, Guan G, Li X, Jagadale A D, Ma X, Wang Z, Hao X, Abudula A. A novel electroactive

654 λ-MnO_2/PPy/PSS core–shell nanorod coated electrode for selective recovery of lithium ions at low

655 concentration. Journal of Materials Chemistry A, 2016, 4(36): 13989-96. doi: 10.1039/c6ta05985f.

656 [17]Tipplook M, Sudare T, Shiiba H, Seki A, Teshima K. Single-Step Topochemical Synthesis of

657 NiFe Layered Double Hydroxides for Superior Anion Removal from Aquatic Systems [J]. ACS

658 Appl Mater Interfaces, 2021, 13(43): 51186-51197.

659 [18]Tian M, Liu C, Neale Z G, Zheng J, Long D, Cao G. Chemically Bonding NiFe-LDH

660 Nanosheets on rGO for Superior Lithium-Ion Capacitors. ACS Appl Mater Interfaces, 2019, 11(39):

661 35977-86. doi: 10.1021/acsami.9b10719.

662 [19]Forticaux A, Dang L, Liang H, Jin S. Controlled synthesis of layered double hydroxide

663 nanoplates driven by screw dislocations. Nano Lett, 2015, 15(5): 3403-9. doi:

664 10.1021/acs.nanolett.5b00758.

665 [20]Ghani M, Ghoreishi S M, Azamati M. Magnesium-aluminum-layered double hydroxide-

666 graphene oxide composite mixed-matrix membrane for the thin-film microextraction of diclofenac

667 in biological fluids. J Chromatogr A, 2018, 1575: 11-7. doi: 10.1016/j.chroma.2018.09.024.

668 [21]He H, Kang H, Ma S, Bai Y, Yang X. High adsorption selectivity of ZnAl layered double

669 hydroxides and the calcined materials toward phosphate. J Colloid Interface Sci, 2010, 343(1): 225-

670 31. doi: 10.1016/j.jcis.2009.11.004.

671 [22]Abo El-Reesh G Y, Farghali A A, Taha M, Mahmoud R K. Novel synthesis of Ni/Fe layered

672 double hydroxides using urea and glycerol and their enhanced adsorption behavior for Cr(VI)

removal. Sci Rep, 2020, 10(1): 587. doi: 10.1038/s41598-020-57519-4.

[23]Cao L, Ma Y, Song A, Bai L, Zhang P, Li X, Shao G. Stable composite of flower-like NiFe-layered double hydroxide nucleated on graphene oxide as an effective catalyst for oxygen reduction reaction. International Journal of Hydrogen Energy, 2019, 44(12): 5912-20. doi: 10.1016/j.ijhydene.2019.01.075.

[24]Zhao G, Li C, Wu X, Yu J, Jiang X, Hu W, Jiao F. Reduced graphene oxide modified NiFe-calcinated layered double hydroxides for enhanced photocatalytic removal of methylene blue. Applied Surface Science, 2018, 434: 251-9. doi: 10.1016/j.apsusc.2017.10.181.

[25]Zhao X J, Zhu Y Q, Xu S M, Liu H M, Yin P, Feng Y L, Yan H. Anion exchange behavior of M(II)Al layered double hydroxides: a molecular dynamics and DFT study. Phys Chem Chem Phys, 2020, 22(35): 19758-68. doi: 10.1039/d0cp02537b.

[26]He X, Cao L, He G, Zhao A, Mao X, Huang T, Li Y, Wu H, Sun J, Jiang Z. A highly conductive and robust anion conductor obtainedviasynergistic manipulation in intra- and inter-laminate of layered double hydroxide nanosheets . Journal of Materials Chemistry A, 2018, 6(22): 10277-10285. doi: 10.1039/c8ta02193g.

[27]Morimoto K, Anraku S, Hoshino J, Yoneda T, Sato T. Surface complexation reactions of inorganic anions on hydrotalcite-like compounds. J Colloid Interface Sci, 2012, 384(1): 99-104. doi: 10.1016/j.jcis.2012.06.072.

[28]Chen J, Fan X, Ji X, Gao T, Hou S, Zhou X, Wang L, Wang F, Yang C, Chen L, Wang C. Intercalation of Bi nanoparticles into graphite results in an ultra-fast and ultra-stable anode material for sodium-ion batteries. Energy & Environmental Science, 2018, 11(5): 1218-25. doi: 10.1039/c7ee03016a.

695 [29]Yang Y, Xie Y, Yu Z, Guo S, Yuan M, Yao H, Liang Z, Lu Y R, Chan T-S, Li C, Dong H, Ma S.

696 Self-supported NiFe-LDH@CoSx nanosheet arrays grown on nickel foam as efficient bifunctional

697 electrocatalysts for overall water splitting. Chemical Engineering Journal, 2021, 419:129512. doi:

698 10.1016/j.cej.2021.129512.

699 [30]Hao X, Yan T, Wang Z, Liu S, Liang Z, Shen Y, Pritzker M. Unipolar pulse electrodeposition of

700 nickel hexacyanoferrate thin films with controllable structure on platinum substrates. Thin Solid

701 Films, 2012, 520(7): 2438-48. doi: 10.1016/j.tsf.2011.10.005.

702 [31]Youmbi B S, Pélisson C-H, Denicourt-Nowicki A, Roucoux A, Greneche J-M. Impact of the

703 charge transfer process on the Fe^{2+}/Fe^{3+} distribution at Fe_3O_4 magnetic surface induced by deposited

704 Pd clusters. Surface Science, 2021, 712:121879. doi: 10.1016/j.susc.2021.121879.

705 [32]Wan J, Wu B, Lo I M C. Development of Fe^0/Fe_3O_4 composites with tunable properties

706 facilitated by Fe^{2+} for phosphate removal from river water. Chemical Engineering Journal, 2020,

707 388:124242. doi: 10.1016/j.cej.2020.124242.

708 [33]He Y, Lin H, Dong Y, Li B, Wang L, Chu S, Luo M, Liu J. Zeolite supported Fe/Ni bimetallic

709 nanoparticles for simultaneous removal of nitrate and phosphate: Synergistic effect and mechanism.

710 Chemical Engineering Journal, 2018, 347: 669-81. doi: 10.1016/j.cej.2018.04.088.

711 [34]Ji W, Niu J, Zhang W, Li X, Yan W, Hao X, Wang Z. An electroactive ion exchange hybrid

712 film with collaboratively-driven ability for electrochemically-mediated selective extraction of

713 chloride ions. Chemical Engineering Journal, 2022, 427. doi: 10.1016/j.cej.2021.130807.

714

715

716

717

718

719

720

721